

Multi-wavelength operation and vertical emission in THz quantum-cascade lasers*

Giacomo Scalari,^{a)} Lorenzo Sirigu,^{b)} Romain Terazzi, Christoph Walther, Maria I. Amanti, Marcella Giovannini, Nicolas Hoyler, and Jérôme Faist
Institute of Physics, University of Neuchâtel, CH-2000 Neuchâtel, Switzerland

Marcin L. Sadowski
GHMFL, Grenoble High Magnetic Field Laboratory, Grenoble, France

Harvey Beere and David Ritchie
Cavendish Laboratory, University of Cambridge, Cambridge, United Kingdom

L. Andrea Dunbar and Romuald Houdré
Institute of Photonics and Quantum Electronics, Swiss Federal Institute of Technology Lausanne-EPFL, CH-1015 Lausanne, Switzerland

(Received 25 July 2006; accepted 12 October 2006; published online 27 April 2007)

Multi-wavelength laser action in the terahertz (THz) region from a quantum cascade structure is demonstrated. Laser emission is obtained at 1.39 and 2.3 THz by using a structure based on a large single quantum well. A strong perpendicular magnetic field is employed to increase the gain and achieve laser action. In the second part of the work, a vertically emitting THz quantum cascade laser device that exploits an in-plane optical resonator based on a two-dimensional photonic crystal is demonstrated. Stable single mode vertical emission is reported. Simulations based on the block-iterative frequency-domain method on a plane wave basis account for the observed results.
 © 2007 American Institute of Physics. [DOI: 10.1063/1.2723183]

I. INTRODUCTION

Quantum cascade lasers (QCL)¹ are unipolar semiconductor laser devices that rely on intersubband electronic transitions in quantum wells. The versatility of these lasers in the far-infrared^{2,3} window of the electromagnetic spectrum has attracted an increasing interest in the last few years, due to the great potentialities of THz radiation in applications such as biomedical imaging and homeland security.⁴ Two key features of intersubband transitions are the absence of reabsorption for photon energies both below and above the transition energy and the intrinsic transverse magnetic (TM) polarization of the emitted photons due to the breaking of the translational invariance of the crystal in the growth direction.⁵ The absence of reabsorption for widely spaced photon energies make intersubband devices ideal systems for multifrequency operation and nonlinear optics.⁶ On the other hand, TM polarization hinders vertical emission: this fact calls for an advanced engineering of the optical resonator in order to achieve vertical extraction that is attractive for a multiple integration and miniaturization of laser sources.⁷

In this work we will present a study on a multi-wavelength QCL operating at 1.39 and 2.3 THz in a strong magnetic field and the possibility to achieve vertical emis-

sion from a QCL by means of an optical cavity formed by a two-dimensional photonic crystal operating at 3.7 THz.

II. TWO COLOR EMISSION AT 1.39 AND 2.3 THZ

Quantum cascade laser multicolor operation has already been achieved by direct generation^{8,9} or by nonlinear optics^{10,11} in the mid-IR spectral region ($\hbar\omega_{LO} < h\nu$). Here we propose to use the energy levels of a wide quantum well to obtain multi-wavelength operation at THz frequencies.¹² The possibility to have dual wavelength operation is very attractive in the THz region for applications like dual wavelength imaging.¹³

Our quantum cascade structure (sample V198) is based on 95 repetitions of a 60.7 nm thick GaAs quantum well followed by an injector region.¹⁴ The exact layer sequence is given in the caption of Fig. 1. A multi-wavelength operation can be achieved by selectively injecting carriers in one of the excited states of this large quantum well. As shown schematically in Fig. 1, we inject carriers in states $|3\rangle$ or $|4\rangle$ by resonant tunneling depending on the applied bias. Emission is then achieved at frequencies corresponding to $|3\rangle \rightarrow |2\rangle$, $|4\rangle \rightarrow |3\rangle$ transitions, respectively. For an applied electric field of 0.72 kV/cm [Fig. 1(a)] the ground state of the injector $|i\rangle$ is aligned with state $|3\rangle$. The calculated energy spacing for the optical transition is $E_{32} = 5.9$ meV corresponding to a frequency of 1.39 THz ($\lambda_{32} = 215 \mu\text{m}$). If the electric field is increased to the value of 1.89 kV/cm [Fig. 1(b)] the state $|i\rangle$ is brought into resonance with level $|4\rangle$. The calculated energy spacing $E_{43} = 8.7$ meV corresponds to a frequency of 2.1 THz ($\lambda_{43} \approx 140 \mu\text{m}$).

*This paper is based on a talk presented by the authors at the 28th International Conference on the Physics of Semiconductors, which was held 24-28 July 2006, in Vienna, Austria. Contributed papers for that conference may be found in "Physics of Semiconductors: 28th International Conference on the Physics of Semiconductors," AIP Conference Proceedings No. 893 (AIP, Melville, NY, 2007); see <http://proceedings.aip.org/proceedings/confproceed/893.jsp>

^{a)}Electronic mail: giacomo.scalari@unine.ch

^{b)}Electronic mail: lorenzo.sirigu@unine.ch

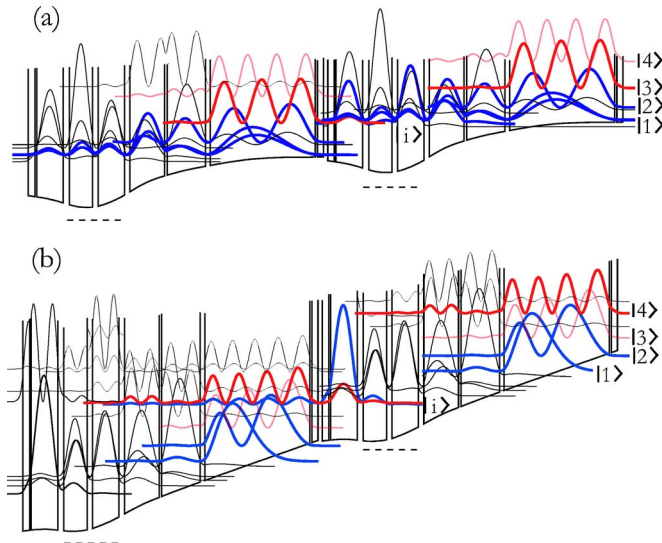


FIG. 1. (Color online) (a): Bandstructure for sample V198 aligned on the $|3\rangle \rightarrow |2\rangle$ transition, for an applied electric field of 0.75 kV/cm. The dashed line highlights the doped region. (b): Bandstructure for sample V198 aligned on the $|4\rangle \rightarrow |3\rangle$ transition, for an applied electric field of 1.89 kV/cm. The layer sequence, starting from the injection barrier is (in nm): **2.5/3.5/1.2/60.7/2.7/22.2/1.5/20.0/3.2/15.2/3.2/13.4/3.5/15.4/1.0/3.8**. The figures in boldface represent the $\text{Al}_{0.15}\text{Ga}_{0.85}\text{As}$ barriers and the underlined layers are doped with Si, $1.6 \times 10^{16} \text{ cm}^{-3}$ in density. This doping level yields a sheet carrier density $n_s = 5.08 \times 10^{10} \text{ cm}^{-2}$.

As recently demonstrated,¹⁵ lateral quantization obtained by means of a magnetic field applied perpendicularly to the plane of the layers greatly enhances the performances of THz intersubband lasers by both reducing the waveguide losses and enhancing the upper state lifetime. The chosen waveguide is the one that employs the second TM mode of a single plasmon waveguide,² already described in Ref. 15. This waveguide presents a figure of merit slightly worse than the double metal one,¹⁶ but has the advantage of a lower reflectivity at the facet. This allows a reasonable out coupling for the laser power that is important when measuring the lasers in the magnetic field, where the optical losses on the light path are relevant.

A plot of the light emission as a function of the applied magnetic field in the 0–12 T interval for sample V198 is reported in Fig. 2. Two distinct regions are evident: At high injection currents ($I > 0.4$ A) and starting from an applied magnetic field value of 3 T a strong laser emission is detected, which indeed corresponds to the $|4\rangle \rightarrow |3\rangle$ transition. At higher magnetic fields ($B > 7$ T) and low injection currents we can observe the laser emission relative to the $|3\rangle \rightarrow |2\rangle$ transition. The light emission has been represented in a logarithmic scale in order to account for the huge intensity variations between the two regions.

Spectral measurement for the $|4\rangle \rightarrow |3\rangle$ transition yield an emission energy of 9.6 meV ($\lambda \approx 130 \mu\text{m}$) depending on the applied magnetic field (see Fig. 2), in reasonable agreement with the calculated value of 8.7 meV. The laser line relative to the $|3\rangle \rightarrow |2\rangle$ transition is centered at 5.9 meV (see spectrum in Fig. 2). The oscillations of laser intensity as a function of the magnetic field are due to lifetime modulations induced by Landau level coupling.¹⁵

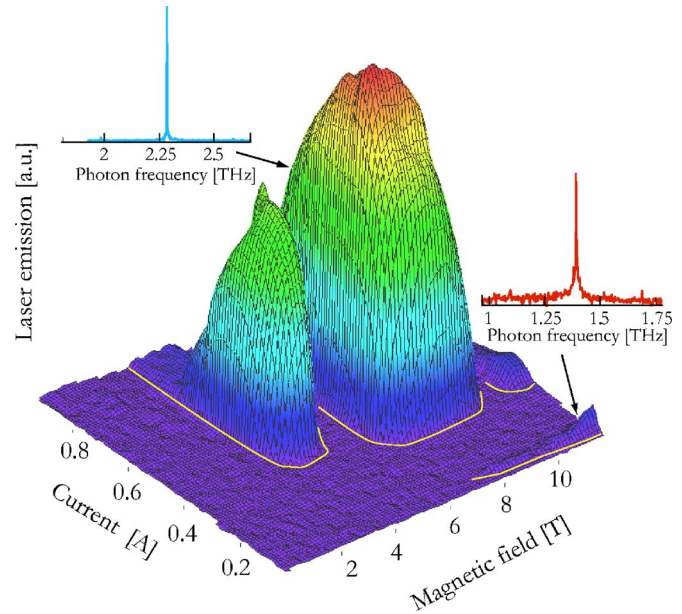


FIG. 2. (Color online) Three-dimensional graph showing laser emission as a function of injected current and applied magnetic field. The logarithm of laser emission has been used in order to enhance the low intensity emission for the laser line at 1.39 THz. The yellow curve tracks the threshold current as a function of the applied magnetic field. The measurements are performed at $T = 4.2$ K.

III. HIGH MAGNETIC FIELD MEASUREMENT AT 1.39 THZ

The same device has been measured also in a very intense magnetic field for the 1.39 THz emission. The lasers are inserted in the bore of a resistive 28 T cw magnetic field solenoid (Grenoble High Magnetic Field Laboratory facility). The electrical and optical characteristics of the laser are recorded while the magnetic field is swept from 0 to 28 T. The emitted power is guided with a light pipe to a Fourier-transform infrared (FTIR) spectrometer equipped with an He-cooled bolometer. The whole light path is kept under vacuum in order to avoid signal absorption from water vapor that can be extremely strong at these low THz frequencies. Laser action is observed starting from 6 T up to the highest magnetic field value of 28 T. A plot of the laser emission as a function of the applied magnetic field for a constant value of the injected current is shown in Fig. 3. Laser emission shows pronounced oscillations as a function of the applied magnetic field. The position of the maxima and the minima is independent from the applied bias. The modulation in the light intensity as a function of the applied magnetic field reflects and analogous modulation of the lifetime of the upper state of the lasing transition. The lifetime modulations are due to the intersubband Landau level resonance phenomena involving one or two electrons depending on the ratio between the energy spacing $E \approx 5.9$ meV and the cyclotron energy $E_c = \hbar\omega_c = \hbar(eB/m^*)$. These intersubband Landau level resonances couple Landau levels of a different index when the system is in the presence of elastic scattering introduced by an interface roughness of impurities. Laser emission shows a maximum for an applied field of 13 T, then it decreases.

The threshold current density as a function of the applied

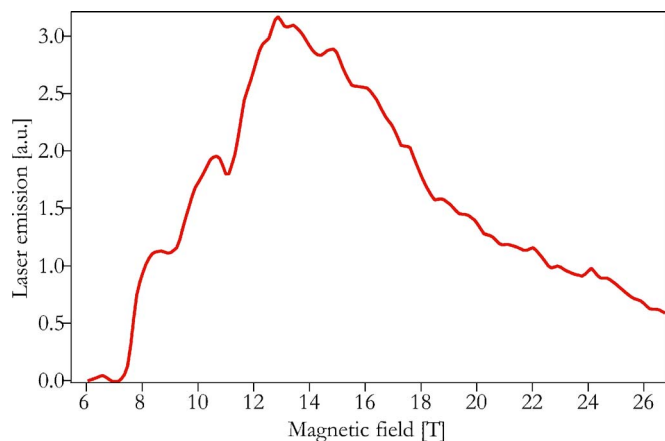


FIG. 3. (Color online) Laser emission as a function of the applied magnetic field for a constant value of the injected current density ($J=15 \text{ A/cm}^2$). The measurement is performed at a temperature $T=4.2 \text{ K}$.

magnetic field is plotted in Fig. 4. As expected from previous research,¹⁵ the threshold current density shows a decreasing behavior with the applied magnetic field, with some local maxima produced by the magneto-intersubband resonances. The value of the threshold current density is extremely reduced, constantly below 6 A/cm^2 for magnetic fields stronger than 10 T . Contrarily to the emitted power, threshold current density shows a monotonous trend after the local maximum at $B=11 \text{ T}$ and shows no particular features in correspondence of the maximum of light emission at $B=13 \text{ T}$. The minimum value at $B=28 \text{ T}$ is 2 A/cm^2 . In the inset of Fig. 4 a spectrum of the laser emission for an applied magnetic field of 28 T is visible. The envelope of the modes of the Fabry-Pérot cavity is centered around $222 \mu\text{m}$, corresponding to a frequency of 1.35 THz .

IV. VERTICAL EMISSION BY PHOTONIC CRYSTAL RESONATOR AT 3.5 THZ

Photonic crystal (PC) structures have acquired an increasing interest over the past few years as versatile photonic

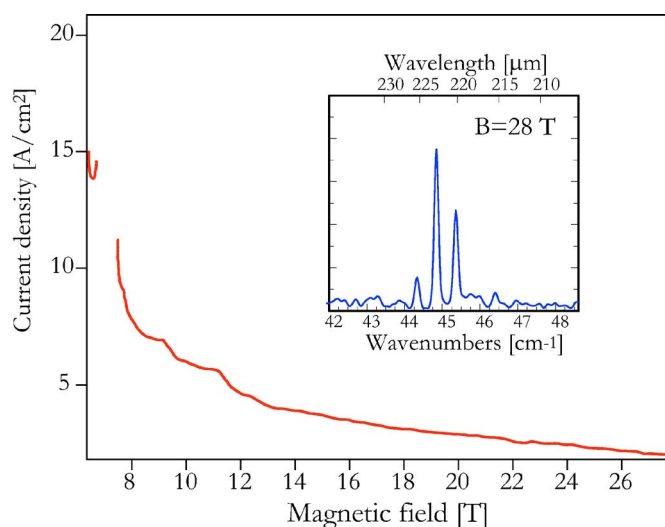


FIG. 4. (Color online) Threshold current density for sample V198 as a function of the applied magnetic field. Inset: Spectrum of a Fabry-Pérot laser cavity for an applied magnetic field of 28 T .

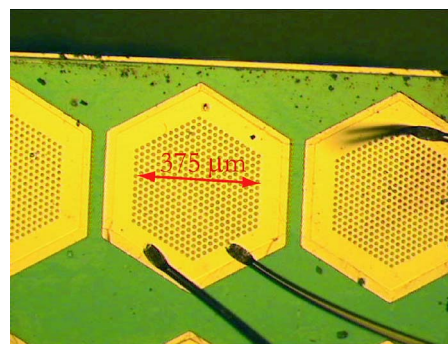


FIG. 5. (Color online) Optical microscope picture of an array of the photonic crystal based vertically emitting THz QCLs.

devices that allow efficient waveguiding, ultrahigh- Q optical cavities, and improved light extraction characteristics. The combination of the photonic flexibility together with the intrinsic wavelength agility of the quantum cascade lasers is, therefore, an attractive approach to follow in order to fabricate mid-infrared or THz laser devices with both a strong spectral selectivity and mode pattern control.^{7,17} In this work, we show a vertically emitting THz quantum cascade laser device that exploits an in-plane optical resonator based on a two-dimensional photonic crystal.

The device is based on a bound-to-continuum active region combined with an optical phonon extraction mechanism.¹⁸ The GaAs/ $\text{Al}_{0.15}\text{Ga}_{0.85}\text{As}$ active layer is grown by molecular beam epitaxy on a semi-insulating GaAs substrate and it was processed in a double-metal waveguide configuration. For the processing of the devices, the epilayer is first metallized with a Ti/Au layer ($5/500 \text{ nm}$) and then bonded to a metallized hosting n -doped GaAs substrate by means of Au/Au thermocompression wafer bonding. The original substrate is then removed by selective wet etching. The etched surface is then passivated with a 100 nm thick Si_3N_4 layer on which hexagonal apertures are opened by dry etching. The device is then completed with the deposition of a patterned Ti/Au layer ($5/200 \text{ nm}$) on the epilayer that acts at the same time as top contact layer and as photonic crystal resonator (see Fig. 5). The photonic crystal is fabricated by opening circular holes in the top metallic contact layer defined by standard lithography and opened by means of lift-off techniques.

The photonic crystal, a triangular lattice of holes in the top metal, enables us to select a few modes of the surrounding cavity that are compatible with the energy dispersion relations of a crystal photon. From a laser device perspective, only the very few modes that both match the energy dispersion of the photonic crystal and the gain bandwidth of the active region, allow laser action. Four different PC parameters are tested in this work, with a hole radius over lattice parameter ratios r/a ranging from 0.258 to 0.286 .

Laser emission is observed from the top surface of all the structures as shown in Fig. 6. The laser threshold shows a sizable current-shift as the PC parameters change, and a minimum is observed at $J_{\text{th}}=300 \text{ A/cm}^2$ for $r/a=0.278$. This value is comparable to standard ridge waveguide lasers based on the same active region. The observed roll-over of the output power for this particular device occurs well before the

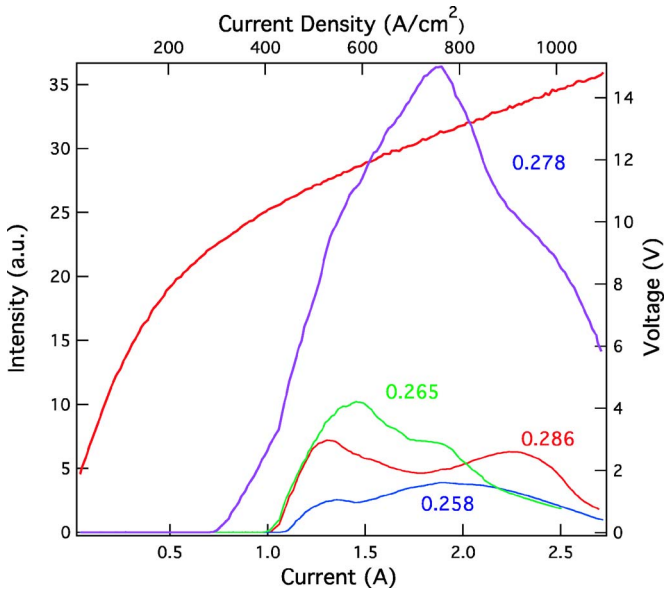


FIG. 6. (Color online) Pulsed LIV curves, with light collected from the top surface of the sample, for four different samples with different PC lattice parameters. On the top of each curve is noted the r/a ratio of the corresponding sample.

negative differential resistance (NDR) regime suggesting an emission cut-off induced by the spectral filtering of the PC resonator. It is worth noting that in our bound-to-continuum active region, laser emission blue-shifts with the applied voltage, due to the Stark effect on a slightly diagonal laser transition. The high frequency selectivity of the PC resonator therefore limits the dynamic range of the laser.

The impact of the photonic crystal resonator on the spectral properties of the laser is shown in Fig. 7. Here we show the spectral evolution observed for a PC parameter $r/a = 0.278$ along the entire dynamic range. The laser emission takes place at 14.9 meV and displays a single mode behavior up to the intensity roll-over. It is worth noting, that this laser

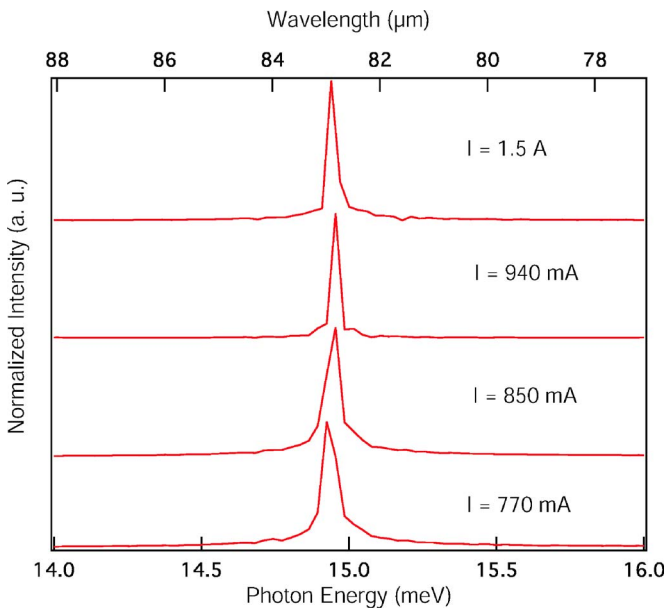


FIG. 7. (Color online) Spectral evolution of a vertically emitting laser device with PC parameters $r/a=0.278$.

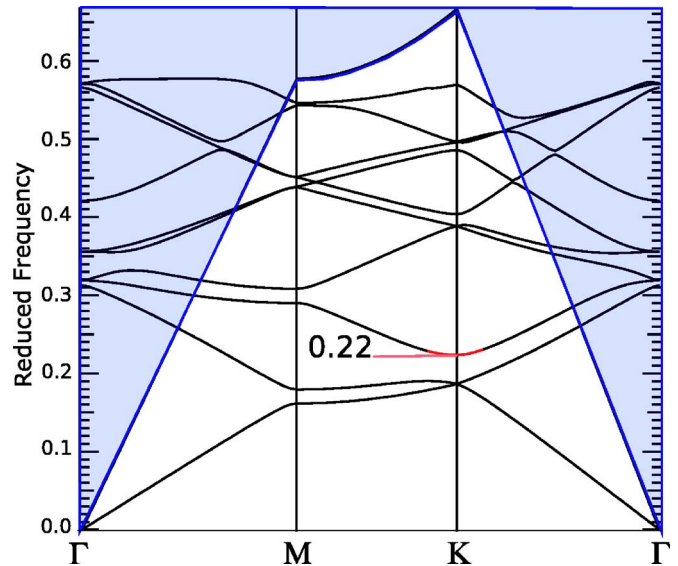


FIG. 8. (Color online) TM photon band diagram of a triangular lattice of holes along $\Gamma MK\Gamma$ path up to the tenth band. The frequency region corresponding to laser wavelength ($\omega=0.22$) is shown. Shaded blue region is the light cone in air.

wavelength is situated on the low energy side of the gain curve of this active region, as witnessed by the saturation of the lasing emission occurring at relatively low operating voltages. This behavior will testify for the strong spectral selectivity of the PC resonator.

In order to elucidate the origin of the spectral features of our device we performed some numerical simulations based on a block-iterative frequency-domain algorithm.¹⁹

The band diagram drawn in Fig. 8 represents the TM photon energy dispersion along the boundary of the first irreducible Brillouin zone ($\Gamma MK\Gamma$ path) of a dielectric triangular lattice of holes. The modal index of a large double metal ridge waveguide (≈ 3.71) is used for the bulk material, while the index in the holes is set to 2.2, corresponding roughly to the modal index of a ridge without the top metal.

The period of the lattice is $a=18 \mu\text{m}$ and the radius of the holes is $r=5 \mu\text{m}$ ($r/a \approx 0.28$). With these parameters, the edge of the third band at the K point overlaps the gain curve of the QC active region for $\omega=0.22$ in reduced frequency units, very close to what is observed experimentally ($\omega=0.216$).

This interpretation is corroborated by measurements of other devices having PC parameters detuned with respect to the K point minimum of the band diagram. Those devices show a laser emission with a multimode spectral behavior due to the poor spectral filtering of the PC at this photon energies.

V. CONCLUSIONS

We demonstrated laser action at two well-separated frequencies from a quantum cascade structure immersed in a magnetic field. The achievement of laser action at very low photon energies ($h\nu=5.9 \text{ meV}$) with extremely reduced threshold current densities is due to the combination of enhanced electron lifetimes and reduced waveguide losses that results from electron localization. Further improvement of

growth technique, quantum design, and optical resonator could allow operation of such low threshold structures even without applied magnetic fields.

For vertical emitting lasers, the effect of the photonic crystal is clearly demonstrated promising further development that includes an operation at other frequencies in the band diagram using different QC active regions. The finite size effect of the photonic structure and the interplay of the surrounding region (cavity effects) also need to be investigated.

ACKNOWLEDGMENT

This work was supported by NCCR-Quantum Photonics and the EU commission through the IST project “Teranova.”

- ¹J. Faist, F. Capasso, D. Sivco, C. Sirtori, A. Hutchinson, and A. Cho, *Science* **264**, 553 (1994).
²R. Köhler, A. Tredicucci, F. Beltram, H. Beere, E. Linfield, A. Davies, D. Ritchie, R. Iotti, and F. Rossi, *Nature* **417**, 156 (2002).
³B. Williams, S. Kumar, Q. Hu, and J. Reno, *Opt. Express* **13**, 3331 (2005).
⁴S. Kim, F. Hatami, J. Harris, A. Kurian, J. Ford, D. King, G. Scalari, M. Giovannini, N. Hoyler, J. Faist *et al.*, *Appl. Phys. Lett.* **88**, 153903 (2006).
⁵A. Tredicucci, *Science* **302**, 1346 (2003).
⁶E. Rosencher, A. Fiore, B. Vinter, V. Berger, P. Bois, and J. Nagle, *Science*

271, 168 (1996).

- ⁷R. Colombelli, K. Srinivasan, M. Troccoli, O. Painter, C. Gmachl, D. Tennant, A. Sergent, D. Sivco, A. Cho, and F. Capasso, *Science* **302**, 1374 (2003).
⁸A. Tredicucci, C. Gmachl, F. Capasso, D. Sivco, A. Hutchinson, and A. Cho, *Nature* **396**, 350 (1998).
⁹C. Gmachl, A. Tredicucci, D. Sivco, A. Hutchinson, F. Capasso, and A. Cho, *Science* **286**, 749 (1999).
¹⁰N. Owschimikow, C. Gmachl, A. Belyanin, V. Kocharovskiy, D. Sivco, R. Colombelli, F. Capasso, and A. Cho, *Phys. Rev. Lett.* **90**, 043902 (2003).
¹¹J. Bengloan, A. Rossi, V. Ortiz, X. Marcadet, M. Calligaro, I. Maurin, and C. Sirtori, *Appl. Phys. Lett.* **84**, 2019 (2004).
¹²C. Sirtori, A. Tredicucci, F. Capasso, J. Faist, D. Sivco, A. Hutchinson, and A. Cho, *Opt. Lett.* **23**, 463 (1998).
¹³D. Chamberlin, P. Robrish, W. Trutna, G. Scalari, M. Giovannini, L. Ajili, J. Faist, H. Beere, and D. Ritchie, *Proc. SPIE* **5727**, 107 (2005).
¹⁴G. Scalari, C. Walthers, J. Faist, H. Beere, and D. Ritchie, *Appl. Phys. Lett.* **88**, 141102 (2006).
¹⁵G. Scalari, S. Blaser, J. Faist, H. Beere, E. Linfield, D. Ritchie, and G. Davies, *Phys. Rev. Lett.* **93**, 237403 (2004).
¹⁶B. Williams, S. Kumar, H. Callebaut, Q. Hu, and J. Reno, *Appl. Phys. Lett.* **83**, 2124 (2003).
¹⁷L. Dunbar, V. Moreau, R. Ferrini, R. Houdré, L. Sirigu, G. Scalari, M. Giovannini, N. Hoyler, and J. Faist, *Opt. Express* **13**, 8960 (2005).
¹⁸G. Scalari, N. Hoyler, M. Giovannini, and J. Faist, *Appl. Phys. Lett.* **86**, 181101 (2005).
¹⁹S. Johnson and J. Joannopoulos, *Opt. Express* **8**, 173 (2001).